Electron transfer complexes in the gut dictate high abundance circulating metabolites

Yuanyuan Liu[1,2], William Van Treuren[2], Bi-Huei Hou[1,2], Steven K. Higginbottom[2], Justin L. Sonnenburg[2,3,4], and Dylan Dodd[1,2†]

[1]Department of Pathology Stanford University School of Medicine, Stanford, CA, USA; [2]Department of Microbiology and Immunology, Stanford University School of Medicine, Stanford, CA, USA; [3]Chan Zuckerburg Biohub, San Francisco, CA, USA; [4]Center for Human Microbiome Studies, Stanford, CA, USA.

[†] Correspondence: ddodd2@stanford.edu

It has long been thought that *Clostridium* and its relatives couple the oxidation of one substrate to the reduction of another, yielding energy in the former step and re-achieving redox balance with the latter. By probing the genetics of reductive metabolic pathways in the gut resident *C. sporogenes*, we find unexpectedly that electron transfer complexes are required for the production of reduced metabolites. Physiologic measurements *in vitro* indicate that the reductive pathways are coupled to ATP formation, revealing that energy is captured not just during substrate oxidation, but also during coupled reduction, accounting for ~40% of the ATP generated in the cell. Electron transfer complex mutants are attenuated for growth in the mouse gut, demonstrating the importance of energy capture during reductive metabolism for gut colonization. Our findings revise a long-standing model for energy capture by *Clostridium* sp., and they reveal that the production of high-abundance molecules by a commensal bacterium within the host gut is linked to an energy yielding redox process.

Proteolytic Clostridia are a group of anaerobic bacteria that have the unique ability to grow with amino acids and peptides as their sole energy source. Early studies with one such bacterium, *Clostridium sporogenes,* revealed that it obtains energy by coupling the oxidation of one amino acid with the reduction of another (the Stickland Reaction)[1]. Oxidative pathways are thought to yield ATP via substrate level phosphorylation, and reductive pathways provide redox balance within the cell[2,3]. However, the ATP yields from oxidative metabolism are modest and cannot fully account for the high growth yields achieved by these bacteria[4-6]. Thus, a key unsolved problem in this area is how bacteria capture energy during Stickland metabolism.

Human feces and isolated microbial strains show prominent metabolic signatures of Stickland metabolism including short-chain fatty acids, branched-chain fatty acids, and aromatic fatty acids, suggesting that these pathways are active in the human gut[7-9]. Stickland metabolites like indolepropionic acid (IPA), indoleacetic acid (IAA), and butyrate are drug-like small molecules that are absorbed into circulation, bind receptors (G-protein coupled receptors and nuclear receptors) and modulate important host processes including intestinal permeability, immune homeostasis, and metabolism[10]. These molecules also mediate syntrophic metabolic interactions, with aryl and branched chain fatty acids being required growth factors for several groups of anaerobic gut bacteria[11-13]. Despite their importance to human health and disease, we know very little about the metabolic processes gut bacteria employ to produce such molecules. Using the gut bacterium *C. sporogenes* as a model, we sought to explore anaerobic amino acid metabolism with an eye toward uncovering mechanisms for energy capture.

C. sporogenes grows rapidly under anaerobic conditions in a defined medium containing a mixture of 23 free amino acids and glucose (1 mM each), achieving a doubling time of ~37 minutes (**Figure 1A**). After 24 h of growth, most amino acids were completely degraded (**Figure 1B**) and a total of fifteen different metabolites that accumulated during growth could be detected by LC-MS or GC-MS in culture supernatants. These compounds include known end products of oxidative (phenylacetate, 4-hydroxyphenylacetate, indoleacetate, acetate, isobutyrate, 2-methylbutyrate, and isovalerate) and reductive Stickland pathways (phenylpropionate, 4-hydroxyphenylpropionate, indolepropionate, 5-aminovalerate, butyrate, and isocaproate) (**Figure 1C**). These findings illustrate the metabolic versatility of *C. sporogenes* and highlight its importance as a model to understand the mechanisms of Stickland metabolism.

To comprehensively assess the degree to which *C. sporogenes* utilizes amino acids as Stickland pairs, we performed a high throughput growth based assay. Pairwise combinations of individual amino acids or glucose (25 mM final concentration each) were made in a basal medium where energy source was limiting. Growth was monitored continuously for 48 h using a microplate spectrophotometer, and the maximum optical density was determined (**Figure 2A**). Results from analysis of the growth data support the following conclusions: 1) The previously unknown Stickland pair, serine/arginine promoted the highest growth yield in *C. sporogenes*. 2) Growth yield from serine was stimulated when combined with reductive pathway substrates (*trans*-4-hydroxyproline (a post-translational modification of proline), proline, tryptophan, histidine, ornithine, and citrulline). 3) Reductive pathway substrates (phenylalanine, tryptophan, proline, *trans*-4-

hydroxyproline, ornithine, citrulline, and arginine) all increased growth yield from glucose. 4) Proline and *trans*-4-hydroxyproline both stimulated growth yield with branched chain amino acids (valine, isoleucine, and leucine), but this required supplemental acetate presumably for carbon assimilation into biosynthetic pathways (**Supplementary Figure 1**). To validate these growth screens, a subset of conditions were performed under more stringent conditions (**Figure 2B**). These experiments revealed particularly large increases in cell yield for the Stickland pairs, valine/proline and serine/arginine (**Figure 2C**). Given existing knowledge of metabolic pathways for arginine[14], valine[5], *trans*-4-hydroxyproline[15], and serine[16] metabolism by *Clostridium* sp., these results support our model for electron transfer between oxidative and reductive pathways (**Figure 2D**).

Having characterized the physiology of Stickland metabolism, we next analyzed the gene clusters that encode these pathways. Unexpectedly, we found that each reductive pathway converged on a step involving a putative electron transfer complex (**Figure 3A**). The aryl amino acid and leucine reductive gene clusters each encoded an acyl-CoA dehydrogenase-EtfAB complex sharing 40-60% amino acid identity with the butyryl-CoA dehydrogenase-EtfAB (Bcd) complex from *Clostridium kluyverii*[17] (**Figure 3B**). Bcd is a recently discovered complex that catalyzes flavin based electron bifurcation where the energetically downhill reduction of crotonyl-CoA by NADH drives the energetically uphill reduction of ferredoxin by NADH[18,19]. In so doing, the cell has low-potential reduced ferredoxin at its disposal to drive electron transport phosphorylation through the Rnf complex with NAD^+ as an electron acceptor[20]. Intriguingly, the proline reductive gene cluster encodes a different electron transfer

complex involving the enzyme proline reductase (**Figure 3C**) which may drive a proline-dependent proton pump in *C. sporogenes*[21]. Cinnamate reductase (**Figure 3D**) is an iron-sulfur flavoenzyme[22] thought to facilitate ATP formation from cinnamate in *C. sporogenes*[6]. Thus, these metabolic gene clusters suggest that reductive Stickland pathways may be linked to ATP synthesis in the cell. To test this experimentally, we established a whole cell-based ATP assay using resting late log phase cell cultures of *C. sporogenes*. Following incubation with substrate, cells were quenched and permeabilized with DMSO, then ATP levels were detected by luminescence and normalized to total protein levels. When pathway intermediates proximal to the electron transfer complexes for Phe, Tyr, Trp, Leu, Pro, and cinnamate were added, ATP levels rose rapidly, plateaued, and then returned to resting levels (**Figure 3E**). For phenylalanine, metabolic profiling revealed that during ATP formation from phenyllactate (**Supplementary Figure 2A**), substrates were quantitatively converted to reductive pathway products (**Supplementary Figure 2B**). Metabolic end products (**Supplementary Figure 2C-D**) or a non-metabolized steroisomer (L-phenyllactic acid) failed to elicit ATP formation (**Supplementary Figure 2E**). Genetic disruption of acyl-CoA dehydrogenase (AcdA), abolished ATP formation from DL-phenyllactic acid, indicating that this enzyme is critical for ATP formation during reductive Phe metabolism (**Supplementary Figure 2F**). Taken together, these experiments reveal that the reductive pathway for Stickland metabolism serves not only to provide redox balance, but also drives ATP formation in the cell.

Having demonstrated that reductive metabolism is coupled to ATP formation, we next asked whether the Rnf complex might be an important coupling site. We identified

a gene cluster which encodes the Rnf complex in *C. sporogenes* (**Figure 4A**) and targeted genes encoding two separate subunits (*rnfB* and *rnfE*) for disruption (**Figure 4B**). These mutants suffered a growth defect when grown in minimal medium containing 10 amino acids (**Figure 4C**), yet this phenotype could be suppressed by the addition of glucose to the culture medium (**Figure 4C**). These data suggest that the growth phenotype is characterized by defective amino acid metabolism. Metabolic profiling of culture supernatants revealed that the *rnfB* mutant was defective in production of the reductive pathway metabolites phenylpropionate, 4-hydroxyphenylpropionate, indolepropionate, and 5-aminovalerate, suggesting an impairment in reductive Stickland metabolism (**Figure 4D**).

Our findings suggest that disruption of the Rnf complex leads to altered amino acid metabolism in vitro. Next we asked whether energy capture through the Rnf complex was important for competition in the gastrointestinal tract. To test this, germ-free mice were colonized with a 1:1 mixture of WT and *rnfB* mutant cells and the relative proportions of the two strains in feces were determined by Q-PCR over time. The *rnfB* mutant was rapidly outcompeted by the WT strain, becoming nearly undetectable in feces by 7 days post colonization (**Figure 4E**). This finding was recapitulated in the presence of a more complex defined microbial consortium revealing the Rnf complex as a key fitness determinant for *C. sporogenes* during colonization and persistence in the gastrointestinal tract (**Figure 4F**).

Our results show that *C. sporogenes* and its relatives ferment amino acids through coupled oxidative and reductive pathways, to produce high abundance metabolites known to influence host-microbe interactions in the gut (**Figure 4G**). In

addition to producing ATP via substrate level phosphorylation, these organisms have evolved strategies to harness chemical energy from the reductive pathway to enable energy capture via electron transport phosphorylation. Acyl-CoA dehydrogenases (Bcd/AcdA/AcdB) capture this energy via flavin-based electron bifurcation, where potential energy is carried by reduced ferredoxin which then drives extracellular proton (or sodium ion) transport. A similar mechanism is used by *Acetobacterium woodii* to stimulate growth during caffeate respiration using electrons donated by molecular hydrogen[23]. Homologs of these electron transfer complexes are present in bacteria from 7 unique Phyla, and 37 different families, (**Supplementary Table 2**), suggesting that this mechanism for energy capture is widespread among anaerobic bacteria. By re-evaluating ATP economy in the cell (considerations in **Supplementary Table 1** and **Supplementary Figure 3**), the reductive pathway can account for ~40% of ATP formation from coupled Stickland redox reactions. This revises our understanding of how these anaerobic bacteria achieve such high growth yields during Stickland metabolism. These results also uncover the metabolic strategies of gut microbes that underlie the production of high abundance metabolites that circulate in the human body.

Methods

Bacterial strains and culture conditions. *Clostridium sporogenes* ATCC 15579 was obtained from the American Type Culture Collection (ATCC). It was routinely cultured in reinforced clostridial medium (RCM) at 37 °C in a Coy type B anaerobic chamber under an atmosphere of 5% hydrogen, 10% carbon dioxide, and 85% nitrogen. All manipulations with *C. sporogenes* were performed in the anaerobic chamber with media and plastic ware that had been pre-reduced for at least 24 hours. The *Escherichia coli* CA434 (HB101/pRK24) conjugation host was routinely cultured at 30 °C in LB broth supplemented with tetracycline (12 μg ml^{-1}) to ensure maintenance of the pRK24 plasmid. *E. coli* TG1 was used for routine cloning. Chloramphenicol (25 μg ml^{-1}) was used for selection of pMTL007C-E2 plasmids in *E. coli*. Organisms used in the defined community colonization included: *Clostridium sporogenes* ATCC 15579, *Clostridium scindens* ATCC 35704, *Eubacterium rectale* ATCC 33656, *Bifidobacterium breve* UCC2003, *Edwardsiella tarda* ATCC 23685, *Bacteroides thetaiotaomicron* VPI-5482, and *Bacteroides vulgatus* ATCC 8482.

Plasmid construction and cloning. For specific gene disruptions, we used the Intron targeting and design tool on the ClosTron website (http://www.clostron.com/clostron2.php) using the Perutka algorithm. The intron contained within the pMTL007C-E2 plasmid was retargeted to the specific sites listed in **Supplementary Table 3** and were synthesized by DNA 2.0 (Menlo Park, CA). Sequencing primers were synthesized by IDT DNA Technologies and are listed in **Supplementary Table 3**.

Mutant generation using ClosTron. Intron-retargeted ClosTron plasmid DNA was introduced into *C. sporogenes* by conjugation as described previously[24]. Transconjugants were selected on RCM agar supplemented with D-cycloserine (250 µg ml^{-1}) and thiamphenicol (15 µg ml^{-1}), re-streaked for purity, and individual well-isolated colonies were inoculated into RCM broth (without agar) containing the same antibiotics. After overnight culture, the cells were diluted 10-fold, then 100 µl was spread on an RCM agar plate containing erythromycin (5 µg ml^{-1}). These colonies were picked, re-streaked onto TYG agar plates supplemented with erythromycin and well-isolated colonies were inoculated into TYG broth supplemented with erythromycin. Genomic DNA was isolated from candidate clones using the DNeasy Blood and Tissue Kit from Qiagen with a lysozyme pre-treatment step, and this DNA was used as a template for PCR using gene-specific primers. Primer sets were designed to produce a ~600-bp product for the wild-type and ~2,800-bp product for the mutant containing the intron. When verified mutants were streaked onto TYG plates containing thiamphenicol, no growth was observed, indicating that the pMTL007C-E2 plasmid had been lost.

Quantitative growth curves in batch culture. To characterize the phenotype of mutants, we used a previously described defined minimal medium referred to as standard amino acid complete medium (SACC). The wild-type and mutant *C. sporogenes* were streaked from an anaerobic glycerol stock onto RCM agar plates without or with erythromycin (5 µg ml^{-1}), respectively, and incubated for ~24 h at 37 °C. Individual well-isolated colonies were inoculated into 5 ml of SACC broth supplemented with glucose (10 mM) and were cultured for 24 h at 37 °C. Cells were diluted ~3,000-fold into fresh SACC medium supplemented with glucose and cultured for 15–16 h to

reach late-log phase. Optical densities at 600 nm (OD600 nm) were recorded for cultures, then cells were washed once with SACC, and subcultured in 20 ml of SACC with or without glucose (10 mM) at an OD600 nm of ~0.01 in 50 ml conical tubes. The tubes were incubated at 37 °C inside the anaerobic chamber, and at hourly intervals, 800 µl aliquots were removed from the chamber and OD600 nm readings were recorded using a GENESYS 30 spectrophotometer from Thermo Scientific.

Metabolite analysis by gas and liquid chromatography - mass spectrometry (GC-MS and LC-MS). *Clostridium sporogenes* ATCC 15579 was cultured in SACC medium as described above, then cells were centrifuged (5,000*g*, 10 min, 4 °C) and 500 µl aliquots of supernatant were taken and stored in sealed 2 mL vials at -20 °C until use.

Amino acid analysis by dansyl chloride derivatization. Culture supernatant was diluted 80-fold with LC-MS grade water, then 50 µl of samples or appropriately diluted standards (Sigma AAS18 supplemented with Trp, Asn, Gln, ornithine, *trans*-4-hydroxyproline, and 5-aminovalerate) were combined with 10 µl internal standards ((L-Arginine:HCl(Guanido-15N2), DL-Valine (D8), L-Methionine (Methyl-D3), L-Phenylalanine (D8), L-Leucine (D10), and L-Tyrosine (D7), 10 µM each) in 96-well V-bottom plates from USA scientific. Then 25 µl of 0.1 M sodium tetraborate and 50 µl of dansyl chloride (25 mM in 100% acetonitrile) were added. The solution was mixed five times by pipetting, then incubated at room temperature in the dark for 15 min, mixed by pipetting five times, then incubated for an additional 15 min. The reaction was quenched by the addition of 50 µl 0.5% formic acid, and the plate was centrifuged at 5,000*g* for 15 min at room temperature. One hundred and twenty five microliters were then transferred to a Multiscreen Solvinert Filter Plate 0.45uM (Millipore) placed on top of a 96-well 0.5

225 ml polypropylene microplate (Agilent) which was then centrifuged at 5,000*g* for 5 min at
226 room temperature. A cap mat was placed on the plate, and samples were analyzed by
227 LC-MS using an Agilent 1290 Infinity II UPLC equipped with a Waters BEH C18 1.7-μm
228 particle size C18 column (2.1 × 100 mm) and detected using an Agilent 6545XT Q-TOF
229 equipped with a dual jet stream electrospray ionization source operating under
230 extended dynamic range (EDR 1700 m/z) in positive ionization mode. Eluent A
231 consisted of 0.1% formic acid (v/v) in water and eluent B consisted of 0.1% formic acid
232 (v/v) in 100% acetonitrile. Five microliters of samples were injected via refrigerated
233 autosampler into mobile phase and chromatographic separation at 40 °C was achieved
234 at a flow rate of 0.5 ml min^{-1} using a linear gradient of 5–60% eluent B over 10.25 min.
235 Eluent B was brought to 95% over 2.25 min, held at 95% for 2.5 min, brought to 5%
236 over 0.1 min, and the column was then re-equilibrated at 5% eluent B for 2.9 min.
237 Electrospray ionization parameters included a gas temperature of 325 °C, drying gas
238 flow of 10 l min^{-1}, nebulizer pressure of 20 psi, sheath gas temperature of 400 °C and
239 flow of 12 l min^{-1}, and capillary voltage of 4000 V. MS1 spectra were collected in profile
240 mode, and peak assignments in samples were made based on comparisons of retention
241 times and accurate masses from authentic standards. Amino acids were quantified by
242 isotope-dilution mass spectrometry using L-Phenylalanine (D8) as a suitable internal
243 standard for most analytes.

244 *Aromatic fatty acids by LC-MS.* Culture supernatants or appropriately diluted
245 standards (phenylacetate, phenylpropionate, 4-hydroxyphenylacetate, 4-
246 hydroxyphenylpropionate, indoleacetate, indolepropionate) (100 μl) were combined with
247 450 μl of methanol followed by incubation at room temperature for 5 min and

248 centrifugation at 13,000*g* for 5 min. Subsequently, 200 µl of supernatant was transferred
249 to wells of a 96-well deep block plate and evaporated to dryness using a Biotage
250 Turbovap. Then 200 µl of resuspension solvent (0.1% formic acid (v/v) in water)
251 containing internal standards (100 µM *trans*-cinnamic acid (D7) and 50 µM indoleacetic
252 acid (D5)) was added, compounds were dissolved by vortexing for ~30 s and samples
253 were clarified by filtration through a Multiscreen Solvinert Filter Plate 0.45uM (Millipore)
254 placed on top of a 96-well 0.5 ml polypropylene microplate (Agilent) by centrifugation at
255 5,000g for 5 min at room temperature. A cap mat was placed on the plate, and samples
256 were analyzed by LC-MS using an Agilent 1290 Infinity II UPLC equipped with a Waters
257 BEH C18 1.7-µm particle size C18 column (2.1 × 100 mm) and detected using an
258 Agilent 6545XT Q-TOF equipped with a dual jet stream electrospray ionization source
259 operating under extended dynamic range (EDR 1700 m/z) in negative ionization mode.
260 Eluent A consisted of 6.5 mM ammonium bicarbonate in water and eluent B consisted
261 of 6.5 mM ammonium bicarbonate in 100% methanol. Five microliters of samples were
262 injected via refrigerated autosampler into mobile phase and chromatographic separation
263 was achieved at a flow rate of 0.35 ml min^{-1} using a linear gradient of 0.5–70% eluent B
264 over 4 min. Eluent B was brought to 98% over 0.5 min, held at 98% for 0.9 min, then
265 brought to 0.5% over 0.2 min and the column was re-equilibrated at 0.5% eluent B for
266 3.4 min. Peak assignments in samples were made based on comparisons of retention
267 times and accurate mass-to-charge ratios from authentic standards analyzed under
268 identical conditions. Electrospray ionization parameters included a gas temperature of
269 250 °C, drying gas flow of 6 l min^{-1}, nebulizer pressure of 30 psi, sheath gas
270 temperature of 200 °C and flow of 11 l min^{-1}, capillary voltage of 4000 V, and nozzle

voltage of 1400 V. MS1 spectra were collected in centroid mode, and peak assignments in samples were made based on comparisons of retention times and accurate masses from authentic standards. Aromatic fatty acids were quantified by isotope-dilution mass spectrometry using *trans*-cinnamic acid (D7) or indoleacetic acid (D5) as internal standards.

Short chain fatty acids by GC-MS. Culture supernatants (50 µl) were acidified with 6 M HCl (50 µl), then diluted in LC-MS grade water (150 µl). Organic acids were then extracted with one volume of diethyl ether (250 µl). An aliquot (95 µl) of the organic layer was transferred to a new sealed vial, combined with N-tert-butyldimethylsilyl-*N*-methyltrifluoroacetamide (MTBSTFA, 5 µl) and derivatized at room temperature for 48 h. One microliter was then injected onto an Agilent 7820A gas chromatograph equipped with an Agilent VF-5HT column (30 m x 0.25 mm x 0.1 µm) coupled to an Agilent 5977B mass spectrometer. The inlet was set to 280 °C, and injection occurred in split mode with a ratio of 10:1. Oven conditions were as follows: 50 °C for 2 min, ramped to 70 °C at 10 °C min^{-1}, then ramped to 85 °C at 3 °C min^{-1}, then ramped to 290 °C at 30 °C min^{-1}. The mass spectrometer transfer line was set to 250 °C, and the quadrupole was set at 150 °C. MS data was collected under scan mode from 50 – 300 m/z with a 3 min solvent delay.

High-throughput growth assay. Amino acids stock solutions (50 mM) in water were prepared, filter-sterilized, then brought into the anaerobic chamber and equilibrated for ~48 h. SACC with 10 amino acids (1 mM each) and acetate (40 mM) was distributed into wells of a 96-well deep block plate (1 ml per well) and evaporated to dryness using a Biotage turbovap. Plates were covered in aluminum foil, autoclaved,

294 then brought into the anaerobic chamber and equilibrated for ~24 h. Pairwise
295 combinations of amino acids were prepared by adding 500 µl of each amino acid (or
296 water) to the wells of the autoclaved deepblock 96-well plate containing dehydrated
297 SACC medium. After reconstitution of the salts, 200 µl of medium was transferred to
298 each well of a 96-well plate (Costar flat bottom with lid). *C. sporogenes* cells (late-log
299 phase) were inoculated into the microplate to achieve a starting OD600 nm of ~0.01.
300 The 96-well plate was then placed into a BioTek Powerwave plate reader and every 15
301 min, OD600 nm readings were taken and the plate was shaken on the 'slow' setting for
302 1 min. Within an experiment, technical duplicates were performed and representative
303 data are shown in **Figure 2**. The growth curve was performed a total of two times with
304 supplemental acetate, and once without acetate.

305 ***ATP assay.*** Wild type *C. sporogenes* cells were streaked from an anaerobic
306 glycerol stock onto a TYG (3% w/v tryptone, 2% w/v yeast extract, 0.1% w/v sodium
307 thioglycolate) agar plate and incubated at 37 °C in an anaerobic chamber from Coy
308 Laboratories under an atmosphere of 5% hydrogen, 10% CO2 and 85% N2. After ~24
309 h, a well isolated colony was inoculated into 5 ml of TYG broth and cultured to
310 stationary phase (~24 h). Cells were diluted into 20 ml of TYG broth (1000-fold dilution)
311 and grown to late-log phase of growth (~16 h). The cells were then harvested by
312 centrifugation (5,000*g*, 10 min, 4 °C) and washed twice with 20 ml volumes of pre-
313 reduced phosphate assay buffer (40 mM potassium phosphate, 10 mM magnesium
314 sulfate, pH 7.0). All centrifugation steps were performed outside of the anaerobic
315 chamber, and so to ensure anaerobiosis, 50 ml falcon tubes were tightly capped and
316 care was taken to limit the total amount of time outside of the chamber. After the final

317 wash step, the cell pellet was re-suspended in 1 ml of phosphate assay buffer and
318 incubated at room temperature for 45 min to achieve a resting cell suspension. During
319 this time, 100 µl of cells were seeded into rows of a 96-well microtiter plate (12 wells per
320 condition being tested). Two hundred microliters of pre-reduced 2 mM substrate in
321 phosphate assay buffer, or buffer alone was dispensed into rows of a separate 96-well
322 microplate. At time zero, 100 µl of substrate or buffer was added to the cells and mixed
323 gently by pipetting. At - 5 min, - 1 min, +30 s, +1 min, +2 min, +5 min, +10 min, +20 min,
324 +30 min, +45 min, +60 min, and +90 min, 10 µl of cells were taken and immediately
325 mixed with 90 µl of DMSO to quench the reaction and liberate cellular ATP. The -5 and -
326 1 minute time-points were taken prior to addition of buffer or substrate, so only 5 µl of
327 cell suspension was harvested, and 5 µl of either buffer or substrate was added to the
328 cell-DMSO mixtures to bring the total volume to 100 µl. At the end of the assay, a 50 µl
329 aliquot of cell suspension was taken for subsequent total protein determination. The
330 ATP content from 10 µl aliquots of lysed cells was then detected using a luminescence-
331 based ATP determination kit from Life Technologies and ATP levels were calculated by
332 extrapolation from a calibration curve constructed with known concentrations of ATP.
333 For protein determination, cellular protein was solubilized in NaOH by combining equal
334 volumes of cells and 0.4 M NaOH (50 µl, each) and incubating at 99 °C for 10 minutes.
335 The protein content was then determined using the DC Protein Assay Kit II from BioRad
336 using bovine serum albumin as a standard. ATP levels were expressed as nmol of ATP
337 per mg of total protein.

338 ***Mouse experiments.*** Mouse experiments were performed on gnotobiotic Swiss
339 Webster germ-free mice (male, 6–10 weeks of age, n = 5 per group) originally obtained

340 from Taconic Biosciences maintained in aseptic isolators. Animal experiments were
341 performed following a protocol approved by the Stanford University Administrative Panel
342 on Laboratory Animal Care. For the mono-colonization experiments, mice were
343 colonized with a 1:1 mixture of wild-type and *rnfB* mutant *C. sporogenes* by oral gavage
344 (200 µl, ~1 × 10^7 CFU) and were maintained on standard chow (LabDiet 5k67). For the
345 defined community, mice were first colonized with a mixture consisting of equal volumes
346 from cultures of *Bacteroides thetaiotaomicron* (~16 h overnight culture), *Bacteroides*
347 *vulgatus* (~ 16 h overnight culture), *Edwardsiella tarda* (~ 16 h overnight culture),
348 *Eubacterium rectale* (~24 h overnight culture), *Clostridium scindens* (~30 h culture), and
349 *Bifidobacterium breve* (~24 h overnight culture). After one week, mice were colonized
350 with a 1:1 mixture of wild--type or *rnfB* mutant *C. sporogenes* (200 µl, ~1 × 10^7 CFU)
351 and were maintained on standard chow (LabDiet 5k67). Fresh fecal pellets were
352 collected and stored at -80 °C until DNA extraction was performed. All mouse
353 experiments were conducted under a protocol approved by the Stanford University
354 Institutional Animal Care and Use Committee.

355 ***DNA isolation and Q-PCR.*** Approximately 10-20 mg of feces was added to
356 individual tubes of a DNeasy PowerSoil DNA Isolation Kit (formerly MO BIO) and DNA
357 was extracted using a Retsch MM400 ball mill according to manufacturer's guidelines.
358 DNA quantitation was performed with an Invitrogen Quant-iT broad range dsDNA assay
359 kit. Two primer sets were used, one designed to amplify total *C. sporogenes*, and
360 another specifically targeted to the erythromycin resistance cassette of the *rnfB* mutant
361 (**Supplementary Table 3**). To amplify genomic DNA (gDNA), we used the Brilliant III
362 SYBR kit from Agilent Technologies. Conditions were as follows: 96-well Q-PCR plates,

363 20 µl reactions, primers at 500 nM each, reference dye included, 5 ng DNA per reaction.
364 Amplification was performed in duplicate using a Stratagene Mx3000P with PCR
365 conditions supplied in the Brilliant III SYBR kit. Initial validation plots were performed
366 using eight serial 4-fold dilutions of gDNA from either WT or *rnfB* mutant *C. sporogenes*
367 spanning 50 ng to 3 pg per reaction. The cycle threshold vs. log(input DNA) was plotted
368 and a linear curve fit was applied. Both primers displayed excellent linearity across this
369 range of DNA concentrations (R^2>0.98). For fecal DNA samples, the cycle number at
370 the threshold crossing point was used to calculate the amount of total *C. sporogenes*
371 DNA or *rnfB* mutant DNA using the standard curves. The competitive index was
372 calculated according to equation 1 below:

373 eq (1) $$CI = \frac{(rnfB\ DNA)}{(Total\ DNA - rnfB\ DNA)}$$

374

Data availability. The authors declare that the data supporting the findings of this study are available within the paper and its Supplementary Information.

Acknowledgements

We are grateful to Michael Fischbach, Christopher Walsh, Audrey Southwick and Curt Fischer (Stanford) and Isaac Cann (Illinois) for valuable discussions. We thank Manhong Wu for assistance with amino acid analysis by LC-MS, Michelle St. Onge with help constructing mutants, and Chun-Jun Guo and Ricardo De La Pena for assistance with GC-MS analysis of short chain fatty acids. This work was funded in part by National Institutes of Health grants DK110335 (D.D.), DK101674 (J.L.S.), DK085025 (J.L.S.) and the Chan Zuckerberg Biohub (J.L.S.).

References

1 Stickland, L. H. Studies in the metabolism of the strict anaerobes (genus *Clostridium*): The chemical reactions by which *Cl. sporogenes* obtains its energy. *Biochem J* **28**, 1746-1759 (1934).

2 Barker, H. A. Amino acid degradation by anaerobic bacteria. *Annu Rev Biochem* **50**, 23-40 (1981).

3 Nisman, B. The Stickland reaction. *Bacteriological reviews* **18**, 16-42 (1954).

4 Lovitt, R. W., Morris, J. G. & Kell, D. B. The growth and nutrition of *Clostridium sporogenes* NCIB 8053 in defined media. *The Journal of applied bacteriology* **62**, 71-80 (1987).

5 Lovitt, R. W., Kell, D. B. & Morris, J. G. The physiology of *Clostridium sporogenes* NCIB 8053 growing in defined media. *The Journal of applied bacteriology* **62**, 81-92 (1987).

6 Bader, J. & Simon, H. ATP formation is coupled to the hydrogenation of 2-enoates in *Clostridium sporogenes*. *FEMS Microbiol Lett* **20**, 171-175 (1983).

7 Smith, E. A. & Macfarlane, G. T. Dissimilatory amino acid metabolism in human colonic bacteria. *Anaerobe* **3**, 327-337 (1997).

8 Russell, W. R. *et al.* Major phenylpropanoid-derived metabolites in the human gut can arise from microbial fermentation of protein. *Mol Nutr Food Res* **57**, 523-535 (2013).

9 Van Treuren, W. & Dodd, D. Microbial contribution to the human metabolome: Implications for health and disease. *Annu Rev Pathol* (2019).

10 Lee, W. J. & Hase, K. Gut microbiota-generated metabolites in animal health and disease. *Nat Chem Biol* **10**, 416-424 (2014).

11 Allison, M. J., Bryant, M. P. & Doetsch, R. N. Volatile fatty acid growth factor for cellulolytic cocci of bovine rumen. *Science* **128**, 474-475 (1958).

12 Stack, R. J., Hungate, R. E. & Opsahl, W. P. Phenylacetic acid stimulation of cellulose digestion by *Ruminococcus albus* 8. *Appl Environ Microbiol* **46**, 539-544 (1983).

13 Hungate, R. E. & Stack, R. J. Phenylpropanoic acid: Growth factor for *Ruminococcus albus*. *Appl Environ Microbiol* **44**, 79-83 (1982).

14 Wildenauer, F. X. & Winter, J. Fermentation of isoleucine and arginine by pure and syntrophic cultures of *Clostridium sporogenes*. *FEMS Microbiol Lett* **38**, 373-379 (1986).

15 Huang, Y. Y., Martinez-Del Campo, A. & Balskus, E. P. Anaerobic 4-hydroxyproline utilization: Discovery of a new glycyl radical enzyme in the human gut microbiome uncovers a widespread microbial metabolic activity. *Gut Microbes* **9**, 437-451 (2018).

16 Fonknechten, N. *et al. Clostridium sticklandii*, a specialist in amino acid degradation:revisiting its metabolism through its genome sequence. *BMC Genomics* **11**, 555 (2010).

17 Seedorf, H. *et al.* The genome of *Clostridium kluyveri*, a strict anaerobe with unique metabolic features. *Proceedings of the National Academy of Sciences of the United States of America* **105**, 2128-2133 (2008).

18 Li, F. *et al.* Coupled ferredoxin and crotonyl coenzyme A (CoA) reduction with NADH catalyzed by the butyryl-CoA dehydrogenase/Etf complex from *Clostridium kluyveri*. *Journal of bacteriology* **190**, 843-850 (2008).

19 Buckel, W. & Thauer, R. K. Flavin-based electron bifurcation, a new mechanism of biological energy coupling. *Chem Rev* **118**, 3862-3886 (2018).

20 Herrmann, G., Jayamani, E., Mai, G. & Buckel, W. Energy conservation via electron-transferring flavoprotein in anaerobic bacteria. *Journal of bacteriology* **190**, 784-791 (2008).

21 Lovitt, R. W., Kell, D. B. & Morris, J. G. Proline reduction by *Clostridium sporogenes* is coupled to vectorial proton ejection. *FEMS Microbiol Lett* **36**, 269-273 (1986).

22 Kuno, S., Bacher, A. & Simon, H. Structure of enoate reductase from a *Clostridium tyrobutyricum* (C. spec. La1). *Biol Chem Hoppe Seyler* **366**, 463-472 (1985).

23 Hess, V., Gonzalez, J. M., Parthasarathy, A., Buckel, W. & Muller, V. Caffeate respiration in the acetogenic bacterium *Acetobacterium woodii*: a coenzyme A loop saves energy for caffeate activation. *Appl Environ Microbiol* **79**, 1942-1947 (2013).

24 Dodd, D. *et al.* A gut bacterial pathway metabolizes aromatic amino acids into nine circulating metabolites. *Nature* **551**, 648-652 (2017).

Figures

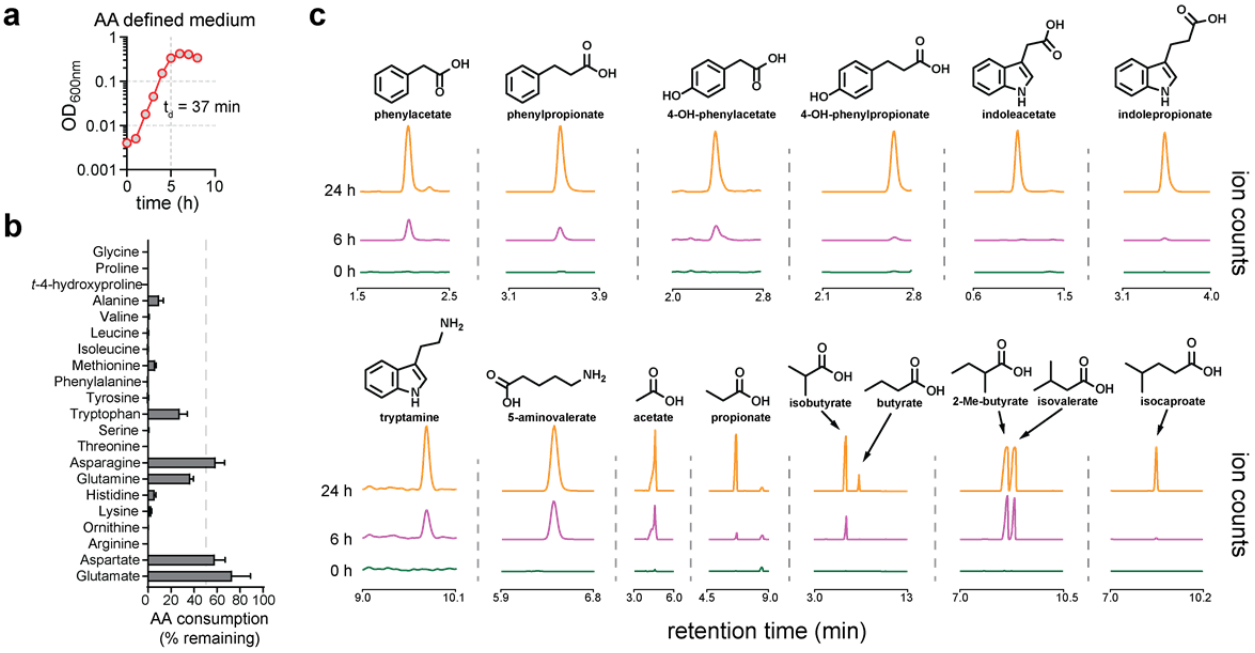

Figure 1. *C. sporogenes* produces fifteen bioactive small molecules during amino acid metabolism. *C. sporogenes* A) grows rapidly in amino acid defined, B) exhibits extensive amino acid degradation, and C) produces fifteen bioactive metabolites. All experiments were repeated independently 3 times. For B, amino acid levels are plotted as means +/- standard deviations from the mean. For A and C, representative data are shown.

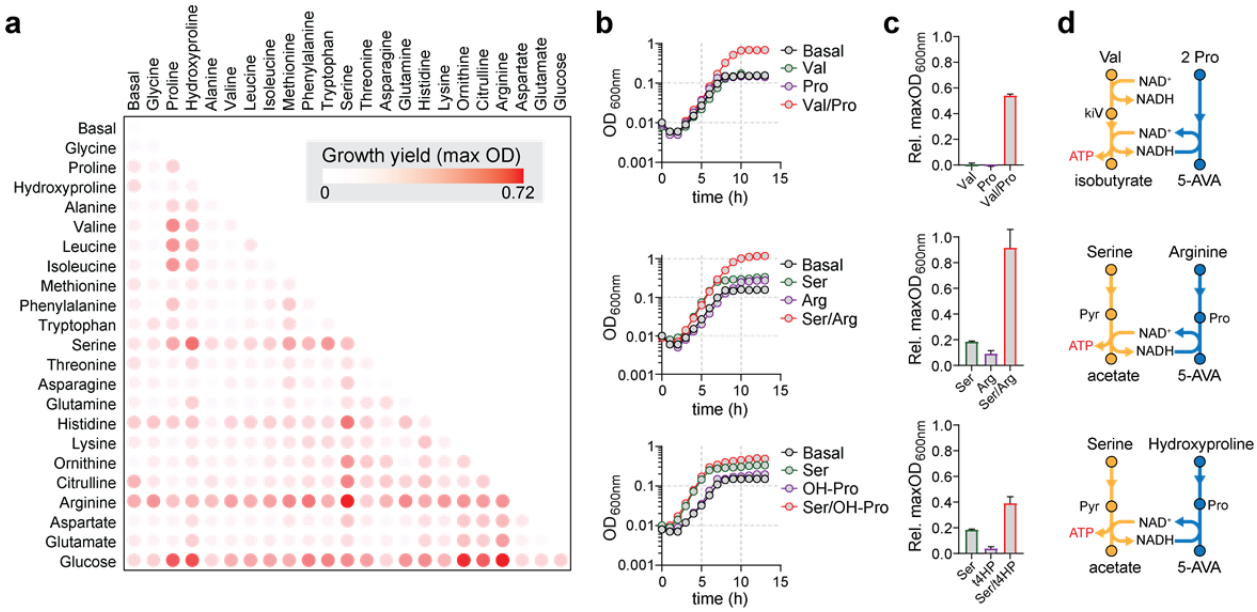

Figure 2. Growth-based assay reveals coupled amino acid metabolism in *C. sporogenes*. A) *C. sporogenes* was grown in basal medium supplemented with acetate (40 mM) and indicated substrates (25 mM) for 48 h and the maximum optical density at 600nm was recorded using a microplate spectrophotometer. B-C) Hit validation in batch culture reveals synergism among specific amino acid pairs. D) Proposed electron transfer between ATP-forming oxidative pathways (yellow) and reductive pathways (blue). In A, the growth screen was performed two times independently with technical duplicates. For B-C, experiments were repeated independently three times. For A-C, representative data are shown.

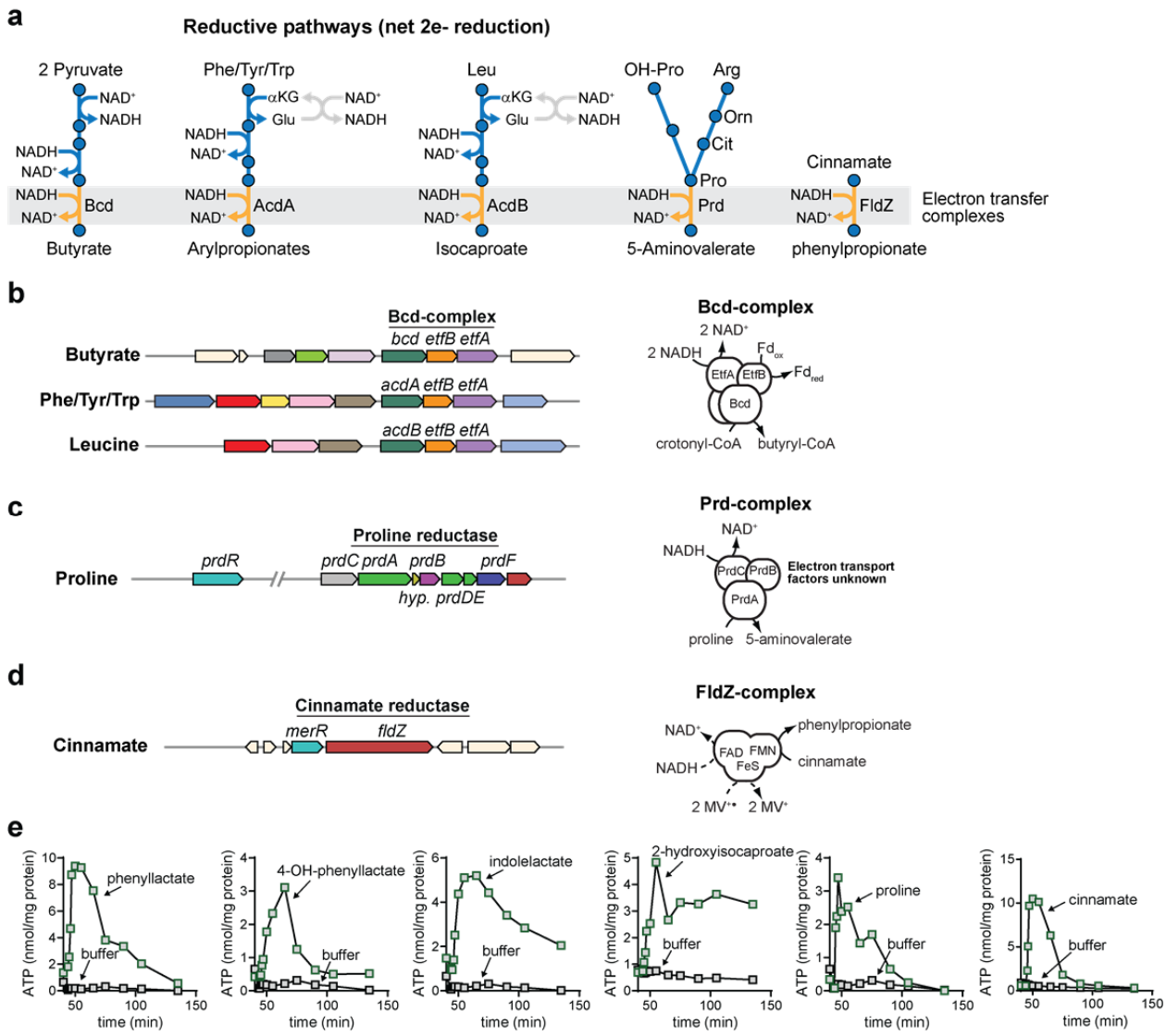

Figure 3. Reductive metabolism is coupled to ATP formation. A) Pathways for reductive Stickland metabolism catalyze net 2 electron reductions and each converges on an electron transfer complex. B) Gene clusters for reductive metabolism of Phe, Tyr, Trp, and Leu all share homologs of the electron bifurcating butyryl-CoA dehydrogenase complex (Bcd) which produces reduced ferredoxin. C) The proline metabolism gene cluster encodes components of the proline reductase enzymes which is implicated in proline-dependent extracellular proton transport. D) The cinnamate reductase gene encodes a unique FAD/[FeS]/FMN containing enzyme with separate binding sites for NADH, cinnamate, and the electron carrier methylviologen (MV). Cinnamate can be reduced by either NADH or $MV^{+\bullet}$. E) Reductive metabolism of Phe, Tyr, Trp, Leu, Pro, and cinnamate are coupled to ATP formation in *C. sporogenes* resting cell suspensions. For E, experiments were repeated independently three times and representative data are shown.

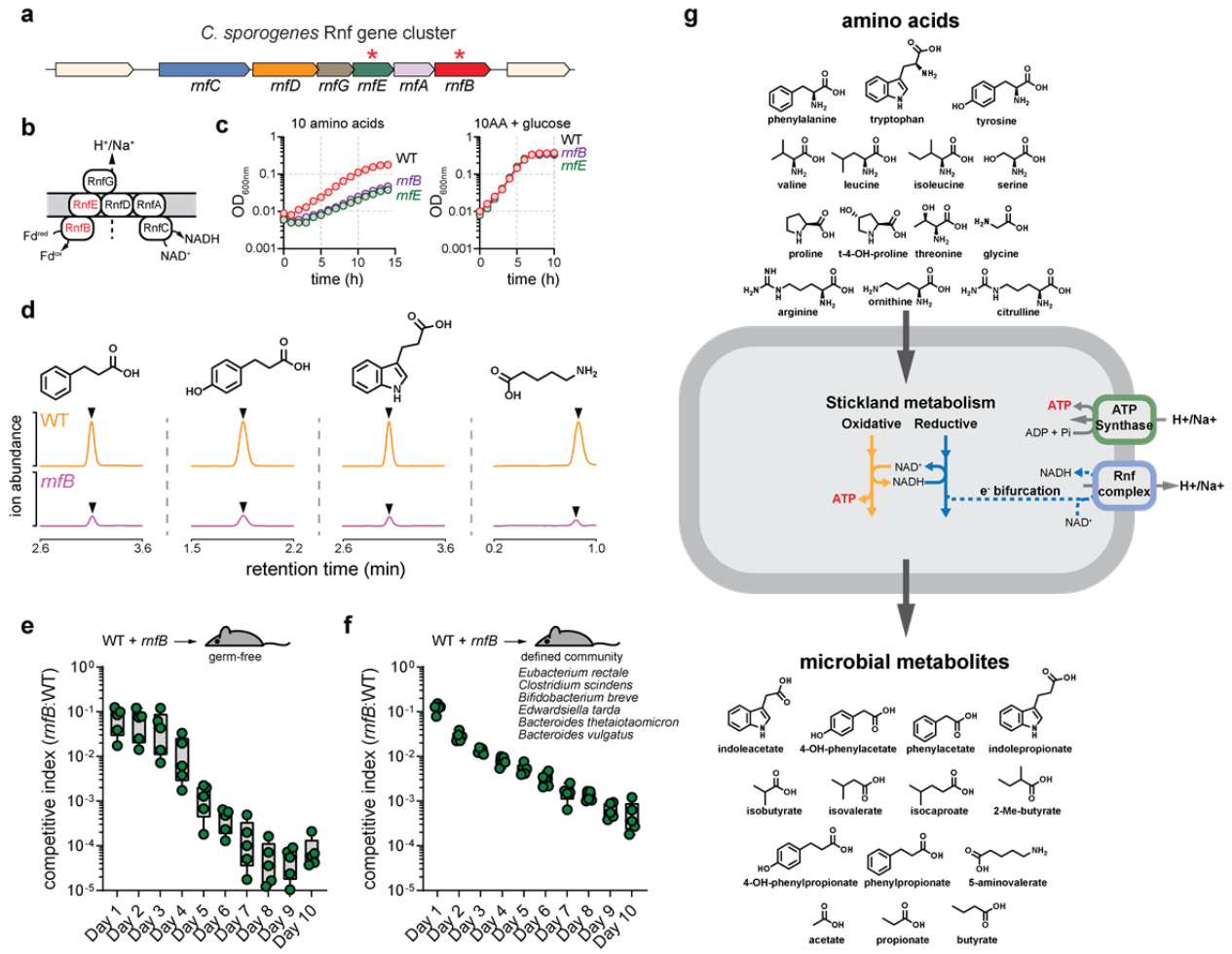

Figure 4. The Rnf complex is important for amino acid metabolism and is a key fitness determinant in vivo. A) The *C. sporogenes* Rnf complex gene cluster. B) Model for the membrane bound Rnf complex which generates a proton or sodium motive force by shuttling electrons from reduced ferredoxin to NAD^+. C) The *rnfB* and *rnfE* mutants suffer a growth defect in amino acid medium that can be restored by glucose. D) The *rnfB* mutant produces less reductive pathway metabolites during growth in defined medium with 10 amino acids. E) The *rnfB* mutant exhibits an in vivo competition defect in gnotobiotic mice in the context of mono-colonization and F) a more complex defined microbial community. G) Revised model for Stickland metabolism and its contribution to gut bacterial derived metabolites. For C-D, experiments were repeated independently three times and representative data are shown. For E-F, Box and whisker plots show median values, 25th–75th percentiles and range for $n = 5$ biological replicates